Molecular Recognition in Nicotinic Acetylcholine Receptors: The Importance of π−Cation Interactions

Jeffrey D. Schmitt,* Christopher G. V. Sharples,§ and W. S. Caldwell

Research and Development, Targacept Inc., Bowman Gray Technical Center, 950 Reynolds Boulevard, Winston-Salem, North Carolina 27105, and School of Biology and Biochemistry, University of Bath, Claverton Down, Bath BA2 7AY, U.K.

Received March 1, 1999

We explore the significance of π−cation interactions in the binding of ligands to nicotinic acetylcholine receptors. Specifically, the Austin method of semiempirical molecular orbital theory is utilized to estimate the interaction of aromatic amino acid side chains with the cation-containing heterocyclic ring fragments of nicotinic ligands. Variational interaction energies (E_i) of side chain−ligand fragment pairs are shown to be distance-dependent and follow a Morse-like potential function. The tryptophan side chain shows the most pronounced interaction with the cation fragments, followed by tyrosine and phenylalanine. For a given side chain, cationic fragments exhibit characteristically different E_i profiles, with the azabicyclo[2.2.1]heptane fragment of the potent nicotinic ligand epibatidine eliciting the greatest interaction energy of the study set. Most significantly, the minimum energy values calculated for numerous fragments correlate with the binding affinity of the parent ligands− we show this to be the case for heteropentameric (α4β2) and homopentameric (α7) nicotinic acetylcholine receptor subtypes. Furthermore, intermolecular distances corresponding to the Morse-like potential minimum also correlate with high-affinity binding. A number of parallel calculations were conducted at the Hartree−Fock 6-31G** ab initio level of theory in an effort to substantiate these findings.

Introduction

Mounting attention has been given to the possible involvement of π−cation interactions in the molecular recognition process (an excellent review of this subject has been published by Dougherty[1]). This theme is of particular interest to the neuroscience community, as the vast majority of neurotransmitters contain cationic moieties. Indeed, sequence and mutagenesis analyses of muscarinic and nicotinic acetylcholine receptors, as well as dopamine and 5-HT receptors, provide evidence that conserved clusters of aromatic amino acids are involved with ligand binding.[2−14] More direct indications of π−cation interactions have been provided by analysis of X-ray crystal structures of a number of proteins, including cytosine-DNA methyltransferase,[15] the phosphocholine-binding antibody McPC603,[16] and acetylcholinesterase.[17] Ordentilch and co-workers have carried out subsequent mutagenesis studies on the acetylcholinesterase active site aromatics Trp-86 and Tyr-133; their results strongly suggest not only a catalytic but also an allosteric function for these residues.[18] A recent NMR study suggests that phenylalanine is responsible for the binding of divalent cations in the active site of tyrosine hydroxylase.[19] Lin and Johnson applied a novel conformational modeling approach to generate inhibitor complexes of the serine protease factor Xa. Their most predictive models cluster three aromatic side chains around the inhibitors, forming a π-rich binding pocket.[20]

The physical basis and mechanism of the π−cation interaction has been explored by a number of chemical and theoretical approaches.[1] Among the earliest theoretical works investigating the biological relevance of π−cation interactions is by Kier and Aldrich[21] who, in the mid-1970s, calculated the interaction energies of a number of amino acid side chains with methylammonium ion and tetramethylammonium ion using a charge-monopole/polarizability-based method.[22,23] Another study having notable impact on biological molecular recognition is a dual crystallography/NMR study of tight association in the tetramethylammonium indole-3-acetylcholine ester.[24] Additionally, Liljefors and Norrby conducted ab initio calculations on G-protein−coupled neurotransmitter receptor ligands. Their results support the primacy of π−cation interactions in this system, although it is possible that aromatic amino acids may function together with anionic amino acids in the binding of ligands.[25] The putative high-affinity binding site of the nicotinic acetylcholine receptor (nAChR) is evidenced to be rich in the aromatic amino acids tyrosine and tryptophan. Site-directed mutagenic substitution of these amino acids or replacement with nonstandard amino acids leads to significant diminution of ligand binding (for a synopsis, see the work of Tsigelny and co-workers[26]). Photoaffinity labeling studies also indicate the presence of high aromatic side chain density at the high-affinity binding site(s).[27−29]

Despite these numerous advances, a quantitative example of a π−cation interaction that correlates directly with biological receptor binding has not been published. Here, we test the hypothesis that aromatic residues in the binding site contribute significantly to the process of cationic ligand recognition and discrimination in the nAChR. Additionally, we postulate binding of a given ligand is correlated with the calculable interaction of the ligand and aromatic amino acid side

* Corresponding author.
§ University of Bath.

10.1021/jm990093z CCC: $18.00
Published on Web 07/24/1999

A

Structure	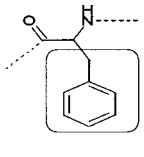	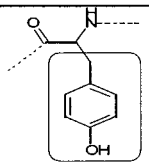	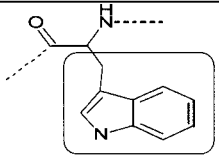	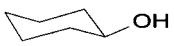
Amino acid Sidechain	Phenylalanine toluene	Tyrosine 4-hydroxytoluene	Tryptophan 3-methyl-1H-indole	– cyclohexanol
Abbreviation	PHE	TYR	TRP	CYCLOHEXANOL

B

Structure	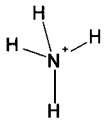	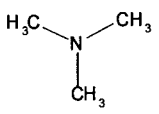	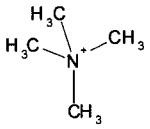	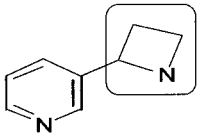
Parent	–	–	–	3-(azetadinyl)pyridine
Fragment	ammonium ion	trimethylamine	tetramethylammonium	azetidine
Abbreviation (protonated)	**1**	–	**3**	**4**
Abbreviation (nonprotonated)	–	**2**	–	**4a**
K_i (nM) α4β2	ND	ND	24[b]	1.1[c]
K_i (nM) α7*	ND	ND	2300	ND
Structure	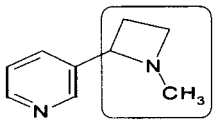	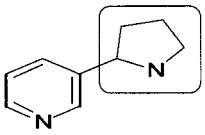	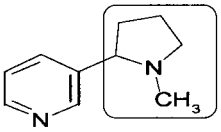	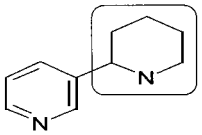
Parent	3-(N-methylazetadinyl)pyridine	nornicotine	nicotine	anabasine
Fragment	N-methylazetidine	pyrrolidine	N-methylpyrrolidine	pipridine
Abbreviation (protonated)	**5**	**6**	**7**	**8**
Abbreviation (nonprotonated)	**5a**	**6a**	**7a**	**8a**
K_i (nM) α4β2	ND	29[b]	4[b]	92[b]
K_i (nM) α7*	ND	730	620	450
Structure	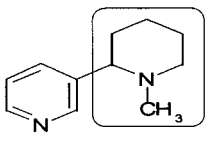	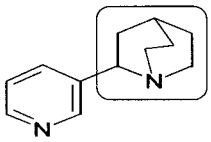	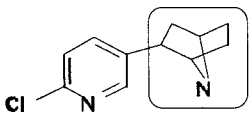	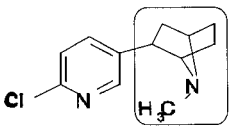
Parent	N-methyl anabasine	RJR-2429	epibatidine	N-methyl epibatidine
Fragment	N-methylpipridine	quinuclidine	azabicyclo[2.2.1]heptane	N-methylazabicyclo [2.2.1]heptane
Abbreviation (protonated)	**9**	**10**	**11**	**12**
Abbreviation (nonprotonated)	**9a**	**10a**	**11a**	**12a**
K_i (nM) α4β2	450[b]	1[b]	0.05[d]	0.26[d]
K_i (nM) α7*	9700	ND	25[e]	ND

Figure 1. Key to molecular structures and biological activities: (A) amino acid side chains (enclosed by boxes) used in energy calculations; (B) cationic ligand fragments (enclosed by boxes) used in energy calculations. Molecular fragments are valence-filled with hydrogen prior to minimization. [a] Displacement of [^{3}H]-α-bungarotoxin using a competition binding assay, ref 38. [b] Displacement of [^{3}H]-*S*(−)-nicotine using a competition binding assay, ref 39. [c] Ref 40. [d] Ref 41.

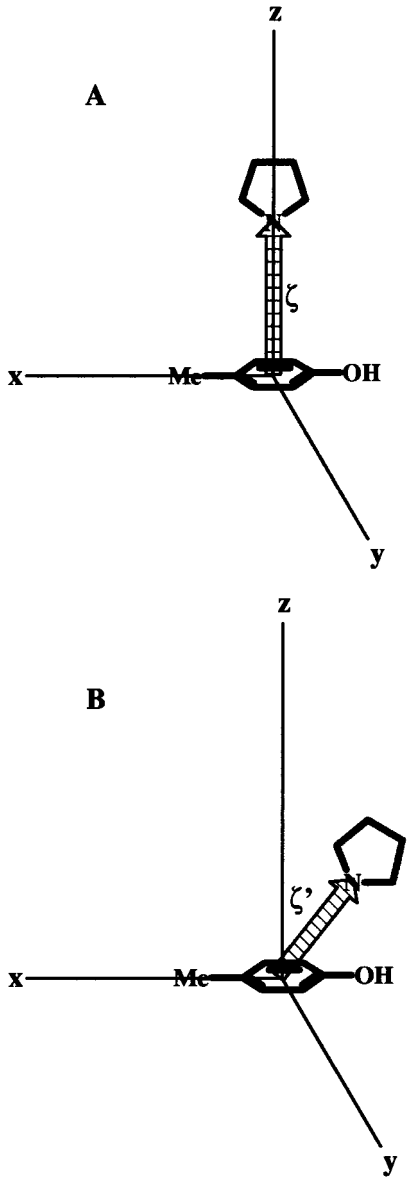

Figure 2. Schematic of side chain−fragment pair geometries: (A) ring-centered approach defined by vector ζ; (B) minimized approach defined by vector ζ'.

chains. In the current work, we sought a compromise between rigor and computational efficiency by using semiempirical molecular orbital theory to probe these putative interactions.

Methods

Restricted Hartree−Fock semiempirical calculations were conducted using MOPAC 6.0,[30] and minimizations were carried out using the method of eigenvector following (EF).[31] The Austin Method Hamiltonian (AM1)[32] was used throughout, although certain calculations were also carried out using the Parametric Method 3 Hamiltonian (PM3)[33] for comparison. Likewise, Spartan[34] was used to conduct ab initio calculations at the Hartree−Fock 6-31G** (HF/6-31G**) level of theory.[35] The Cerius[2] suite of programs was used for all model building and visualization purposes.[36]

In the first experiments, interaction energies were derived by placing fully minimized toluene (the side chain of phenylalanine), 4-hydroxytoluene (the side chain of tyrosine), or 3-methyl-1*H*-indole (the side chain of tryptophan) in an *x*,*y*-plane with the coordinate origin defined as the side chain center-of-mass. See Figure 1 for a key to the structures used in this study. Energies were calculated as the fragments described in Figure 1 were incrementally moved toward the side chain along the *z*-axis. A vector ζ is then defined as the distance between the ligand nitrogen atom and the aromatic ring center-of-mass (Figure 2A); we call this the 'ring-centered approach'. Ligands were oriented on the *z*-axis to both maximize exposure of the cationic nitrogen to the aromatic ring *and* to minimize bad contacts that might arise at small distances.

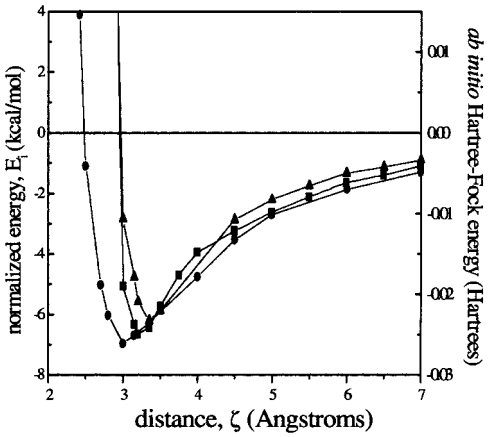

Figure 3. Comparison of semiempirical and ab initio interaction curves for the ligand−side chain pair **11**−Trp: (circles) ab initio HF/6-31G**, (squares) semiempirical AM1, (filled triangles) semiempirical PM3.

The next experiments were aimed at obtaining a preferred orientation of the various pairs before energy calculations. Here, side chain−fragment pairs were placed at 4 Å distances from the aromatic center-of-mass with the nitrogen pointing toward the aromatic moiety center-of-mass and energy-minimized, without positional constraints, using AM1. The approach trajectory for the pair was then defined as the vector ζ_m extending from the side chain center-of-mass to the fragment's nitrogen (as shown in Figure 2B). We call this the 'minimized approach'. Throughout, we define the interaction energy (E_i) using the Rayleigh−Ritz variational principal.[37] Thus, $E_i = E_r - E_{30}$, the heat of formation at a distance r (E_r) minus the heat of formation at an arbitrarily large distance of 30 Å. Energy minima in the E_i versus r profiles are designated E_m. The Rayleigh−Ritz principal is generally accurate in the domain where E_i is not vanishing compared to E_r. Where relevant, the interaction energies were calculated for both protonated and nonprotonated fragments. To be assured that these minimizations converge to the global minima, energy calculations were conducted on a grid lying in the *x*,*y*-plane 4 Å above the plane defined by the aromatic side chain. The ligand orientation was kept constant as it was moved from point to point on the grid. Energy contour plots from two such calculations are shown in Figure 4.

All pharmacological data were either taken from previously published data from our group, from Dr. L. Abood's group,[40] and Dr. S. Wonnacott's laboratory[41] (see the legend of Figure 1). The authors feel justified in using data from these combined sources, since similar equilibrium binding affinity (K_i) values were obtained for a number of representative compounds (data not shown). Binding data (K_i) are divided into two sets for $\alpha 4\beta 2$ correlation: set A (**3, 4, 6, 7, 8, 9, 10, 11, 12**) and set B (**3, 4, 6, 7, 10, 11, 12**). The dataset for $\alpha 7$ binding correlation is designated set C (**3**, **6**, **7**, **8**, **9**, **11**).

Results

HF/6-31G ab initio Energy Profiles Are Approximated by AM1.** Initially we sought to establish that semiempirical methodology would yield results similar to the ab initio for a given side chain−fragment pair. Figure 3 compares E_i as a function of distance for the tryptophan−epibatidine fragment−side chain pair.

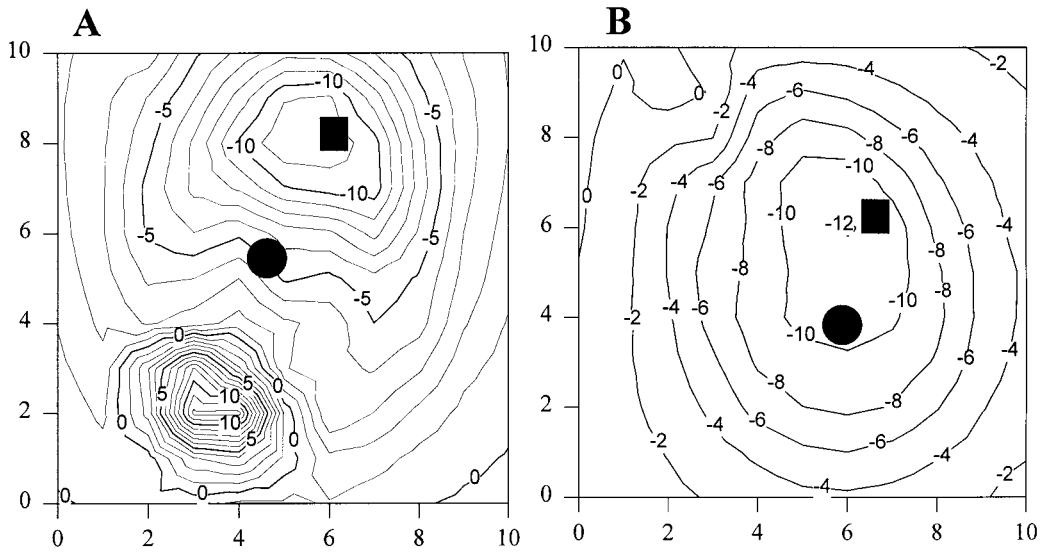

Figure 4. Energy contour graphs generated by moving the protonated epibatidine fragment on a plane 4 Å (divided into a 1 Å grid) above the plane of either the tyrosine side chain (A) or the tryptophan side chain (B). Circles indicate the location of epibatidine's nitrogen in the ring-centered approach (intersection of vector ζ with plane). Squares indicate the location of epibatidine's nitrogen in the minimized approach (intersection of vector ζ′ with plane). Axis units are Angstroms; contour units are kcal/mol.

AM1 and the PM3 Hamiltonian produce nearly identical profiles, although AM1 appears to predict a slightly deeper and wider basin of interaction. While the ab initio calculations yield results that are qualitatively similar to the semiempirical calculations, the ab initio curve predicts that the asymptote due to van der Waals repulsion occurs at smaller intermolecular distances compared to the semiempirical predictions. Additionally, the semiempirical calculations underestimate the extent of favorable interaction energy. This is due to the fact that the 6-31G** basis set contains polarization functions for all atom types, thus allowing for the redistribution of electron density as fragment−side chain pairs approach.

The 'Minimized Approach' Finds the Intermolecular Global Minimum. Here, two initial concerns of this study are addressed: (1) in the ring-centered approach are we generating energy profiles that result from unrealistic constraints on the relative orientation of the side chain−fragment pairs? and (2) in seeking minimized orientations, as with the 'minimized approach', are we finding the global minimum of intermolecular interaction? To resolve these concerns we calculated the energy surface of side chain−fragment pairs on a 2D grid parallel to the aromatic side chain at a distance of 4 Å. Figure 4 shows contour plots of the tyrosine−epibatidine and tryptophan−epibatidine energy surfaces: the circles show the location (i.e. the points where the ζ or ζ′ vectors intersect the *x*,*y*-plane lying 4 Å above the aromatic ring) of the ring-centered approach, and the squares show the location of the minimized approach. In the case of the tryptophan−epibatidine pair, both the ring-centered and the minimized approach trajectories are near the global minimum (Figure 4B). In the case of tyrosine−epibatidine, the ring-centered approach is located near a saddle point 2.4 Å from the global minimum, while the minimized approach is located in the global minimum basin (Figure 4A).

An important qualification must be made in the context of interpreting these results. Our usage of 'intermolecular global minimum' implies a minimum energy configuration between the fragments and the amino acid side chains, where the cationic nitrogen points toward the aromatic ring in a sterically unhindered manner. Although we started with cationic fragments that were exhaustively minimized, one cannot rule out the existence of lower-energy configurations.

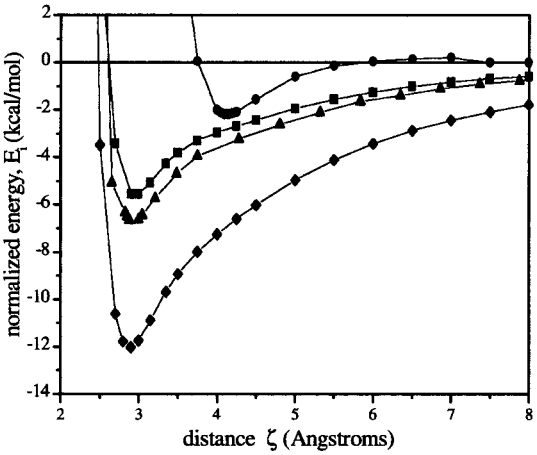

Figure 5. Comparison of semiempirical interaction curves for the fragment **11** and various ligand fragments and the side chains: cyclohexanol (circles), Phe (squares), Tyr (triangles), Trp (diamonds). Energy profiles were derived using the ring-centered approach.

The Azabicyclo[2.2.1]heptane Cation Exhibits Distinct Side Chain Interaction Profiles. Calculated interaction profiles are given (Figure 5) for ligand fragment **11** (azabicyclo[2.2.1]heptane cation) with each of the aromatic amino acid side chains: Phe, Tyr, and Trp. A nonaromatic control, cyclohexanol, is also included to approximate the extent of positive interaction energy that results from heteroatom and/or non-π-related interactions. Figure 5 highlights a consistent observation— for a given cationic fragment, the rank order of interaction energy is Trp > Tyr > Phe > cyclohexanol.

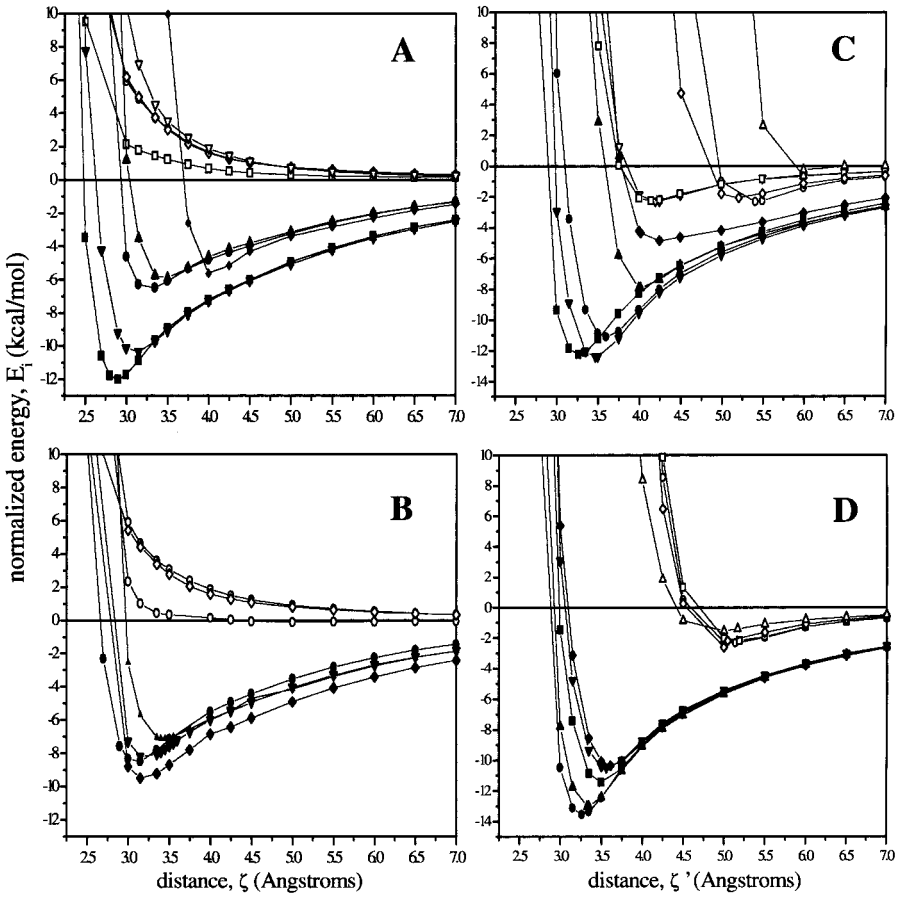

Figure 6. Semiempirical interaction curves for tryptophan: (A, B) ring-centered approach; (C, D) minimized approach. Symbols for panels A and C: **6** (filled down triangles), **6a** (open down triangles), **7** (filled circles), **7a** (open circles), **11** (filled squares), **11a** (open squares), **12** (filled up triangles), **12a** (open up triangles), **3** (filled diamonds), **2** (open diamonds). Symbols for Panels B and D: **9** (filled down triangles), **9a** (open down triangles), **4** (filled circles), **4a** (open circles), **5** (filled squares), **5a** (open squares), **8** (filled up triangles), **8a** (open up triangles), **10** (filled diamonds), **10a** (open diamonds).

Amino Acid Side Chains Possess Distinct Ligand Interaction Profiles. The interaction of ligand fragments with Trp is shown in Figure 6. The ring-centered approach (Figure 6A,B) gives the following rank order of interaction energy (E_m): **11** > **5** ≥ **4** > **6** > **8** = **7** > **12** > **10** ≥ **9** > **3**; the rank order of minimum energy distances (R_m) is: **11** < **4** < **6** = **7** < **5** = **10** = **8** = **9** < **12** < **3**. None of the nonprotonated fragments exhibit favorable (negative) interaction energy as indicated by the ring-centered approach trajectories. The Tyr minimized approach profiles shown in Figure 6C,D reveal deeper basins of interaction for all protonated ligands. The minimized approach gives the following rank order of interaction energy (E_m): **11** > **4** > **6** > **9** > **5** > **10** > **7** > **8** > **12** > **3**; the rank order of minimized R_m distances is: **11** < **4** < **10** = **9** < **5** < **8** ≤ **6** < **7** < **12** < **3**. Interestingly, all of the nonprotonated fragments, with the exception of **12a**, exhibit ≫2 kcal/mol of favorable interaction energy.

The interaction of ligand fragments with Tyr is shown in Figure 7. The ring-centered approach (Figure 7A,B) gives the following rank order of interaction energy (E_m): **11** > **6** > **10** > **4** > **9** > **5** > **8** > **7** > **12** > **3**; the rank order of R_m distances is: **11** < **6** < **4** ≤ **5** < **10** < **9** < **7** < **8** < **12** < **3**. The minimized approach, shown in Figure 7C,D, gives the following rank order of interaction energy (E_m): **4** > **8** > **6** > **11** > **5** > **7** > **10** > **9** > **12** > **3**; the rank order of minimized R_m distances is: **11** = **4** < **8** < **6** < **5** < **9** < **7** ≤ **10** < **3** = **12**. As with the case of the minimized Tyr profiles, we observe a number of nonprotonated fragments (**2**, **4a**, **5a**, **6a**, **8a**) giving negative, albeit small, interaction energies.

The interaction of ligand fragments with Phe is shown in Figure 8. The ring-centered approach (Figure 8A,B) gives the following rank order of interaction energy (E_m): **11** > **4** > **6** > **5** > **10** > **7** > **3** > **12**; the rank order of R_m distances is: **11** < **4** = **5** = **6** < **10** < **7** = **12** < **3**. In contrast to the heteroatom-containing side chains, minimized nonprotonated fragment Phe pairs do not exhibit any favorable interaction energy (data not shown).

Summarized R_m and E_m values for the profiles shown in Figures 6−8 are given in Table 1. N-Methylation of the various ligand fragments leads to a consistent but small diminution of interaction energy. In all cases (**6**→**7**; **8**→**9**; **11**→**12**) we observe a decrease in E_m for both ring-centered and minimized approaches with the exception of two cases: minimized Tyr:**8**→**9** and ring-centered Trp:**8**→**9**. The seemingly ubiquitous effect of N-methylation may be spurious, because, as mentioned before, one cannot rule out the possibility that the optimum configurations of these systems have not been found.

Ligand Fragments Minimize with Bias Toward the Side Chain Heteroatom. The minimization of ligand fragments with heteroatom containing side chains (Tyr, Trp) results in movement of the protonated nitrogen toward the heteroatom of the side chain,

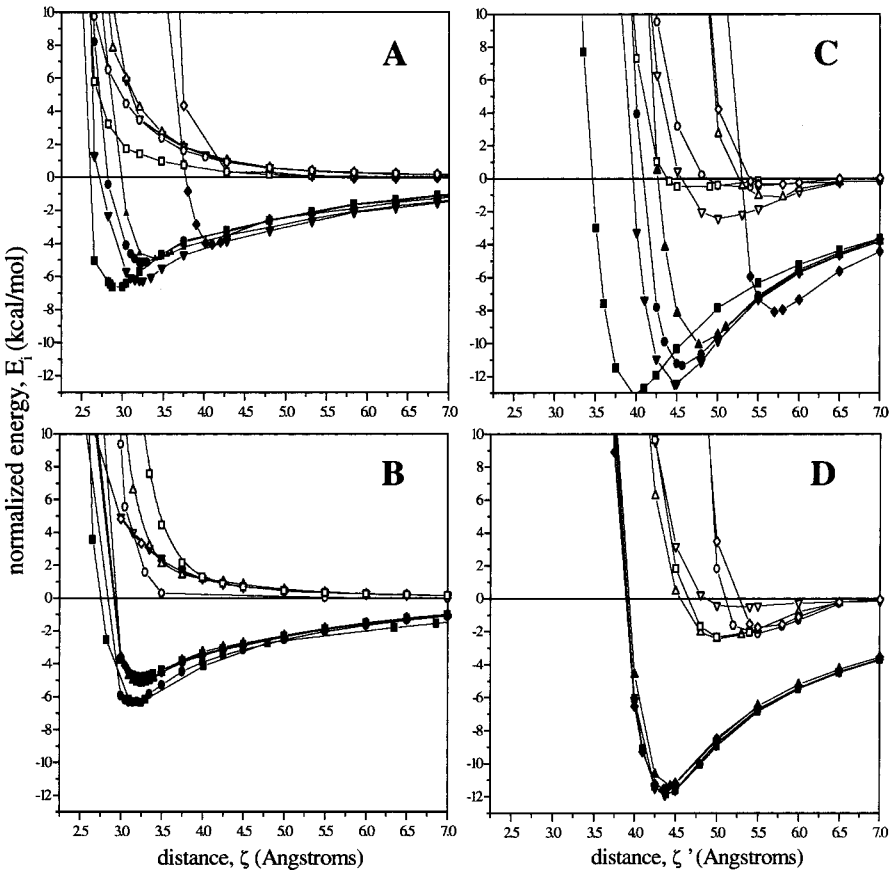

Figure 7. Semiempirical interaction curves for tyrosine: (A, B) ring-centered approach; (C, D) minimized approach. Symbols for panels A and C: **6** (filled down triangles), **6a** (open down triangles), **7** (filled circles), **7a** (open circles), **11** (filled squares), **11a** (open squares), **12** (filled up triangles), **12a** (open up triangles), **3** (filled diamonds), **2** (open diamonds). Symbols for panels B and D: **9** (filled down triangles), **9a** (open down triangles), **4** (filled circles), **4a** (open circles), **5** (filled squares), **5a** (open squares), **8** (filled up triangles), **8a** (open up triangles), **10** (filled diamonds), **10a** (open diamonds).

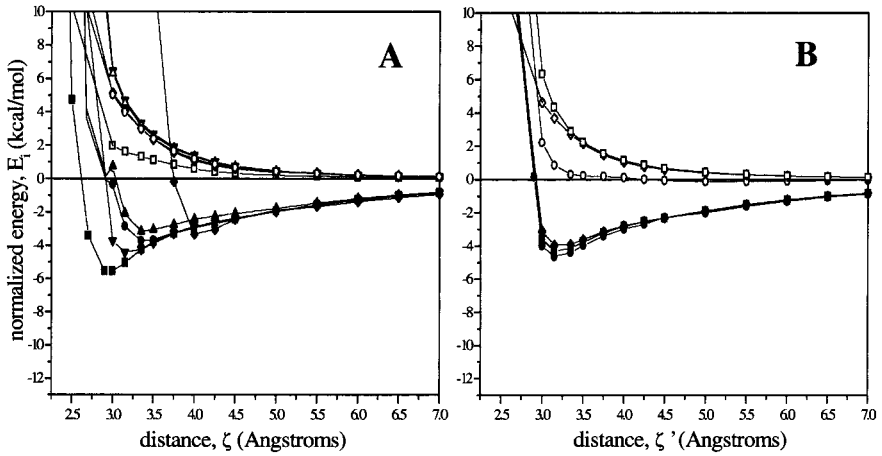

Figure 8. Semiempirical interaction curves for phenylalanine: (A, B) ring-centered approach. Symbols for panel A: **6** (filled down triangles), **6a** (open down triangles), **7** (filled circles), **7a** (open circles), **11** (filled squares), **11a** (open squares), **12** (filled up triangles), **12a** (open up triangles), **3** (filled diamonds), **2** (open diamonds). Symbols for panel B: **9** (filled down triangles), **9a** (open down triangles), **4** (filled circles), **4a** (open circles), **5** (filled squares), **5a** (open squares), **8** (filled up triangles), **8a** (open up triangles), **10** (filled diamonds), **10a** (open diamonds).

possibly as a result of favorable electrostatic interaction. Figure 9A and 9B shows orthogonal views of the minimized approach pairs **11**−Tyr and **10**−Tyr at a distance of $\zeta' = 4$ Å. Both **11**−Tyr (purple) and **10**−Tyr (green) occupy the same region although the fragment **11** is located closer to the aromatic ring center. A plausible explanation for the extent of movement toward the aromatic heteroatom is the subject of further study, although we found no correlation with nAChR binding or a number of different physiochemical parameters (data not shown).

***E*$_m$ and *R*$_m$ Correlate with Equilibrium Binding Affinity.** Here we ask if the variational energy of interaction, E_m, reflects a given ligand's ability to bind (measured by K_i) to the receptor. Linear correlation coefficients were calculated for K_i versus E_m; results are summarized in Table 2. These results indicate a strong correlation between these variables. The possibility of

Table 1. Variational Energy and Minimum Distance Values for Ligand−Fragment Pairs[a]

	Tyr				Trp				Phe	
	ring-centered		minimized		ring-centered		minimized		ring-centered	
ligand	R_m	E_m	R_m	E_m	R_m	E_m	R_m	E_m	R_m	E_m
1	3.10	−10.34	3.96	−17.58	3.00	−11.87	3.26	−17.29	3.05	−7.16
2	4.10	−4.06	5.70	−8.07	4.05	−5.67	4.02	−4.37	4.05	−3.40
3	3.15	−6.33	4.31	−12.76	3.13	−8.54	3.26	−13.58	3.20	−4.64
4	3.25	−6.35	4.39	−11.87	3.15	−7.71	3.50	−11.44	3.20	−4.33
5	3.20	−6.26	4.48	−12.44	3.10	−10.40	3.47	−12.43	3.20	−4.45
6	3.20	−5.15	4.57	−11.35	3.30	−6.56	3.60	−11.12	3.40	−3.74
7	3.25	−5.16	4.44	−11.34	3.40	−7.12	3.33	−13.03	ND	ND
8	8.25	−4.79	4.37	−11.90	3.25	−8.21	3.56	−10.51	ND	ND
9	3.25	−4.88	4.36	−11.53	3.20	−9.52	3.61	−10.56	3.25	−4.02
10	2.90	−6.65	3.97	−13.03	2.90	−12.02	3.26	−12.28	2.95	−5.60
11	3.40	−4.92	4.77	−10.08	3.45	−5.95	4.02	−7.96	3.40	−3.20
2a	ND	ND	5.80	−0.40	ND	ND	5.50	−1.80	ND	ND

[a] R_m values are in Angstroms; E_m values are in kcal/mol; ND, not determined.

Table 2. Correlation between nAChR Ligand Binding and Variational Indices E_m and R_m

		correlation coefficient (r) values				
		Tyr		Trp		Phe
	data set	ring-centered	minimized	ring-centered	minimized	ring-centered
log K_i(α4β2) vs E_m	A	0.655 (1.998[a])	0.613 (2.756)	0.369 (3.462)	0.754 (2.295)	0.833 (1.899)
log K_i(α4β2) vs E_m	B	0.804 (0.735)	0.804 (1.106)	0.525 (2.111)	0.833 (0.980)	ND
log K_i(α4β2) vs R_m	A	0.755 (1.898)	0.716 (1.342)	0.506 (2.315)	0.468 (2.086)	0.483 (2.239)
log K_i(α4β2) vs R_m	B	0.730 (1.210)	0.730 (1.894)	0.678 (1.871)	0.480 (1.198)	ND
log K_i(α7) vs E_m	C	0.774 (1.774)	0.939 (0.401)	0.602 (2.009)	0.977 (0.833)	0.649 (0.998)
log K_i(α7) vs R_m	C	0.979 (0.750)	0.958 (0.668)	0.921 (0.917)	0.934 (0.881)	0.695 (1.312)

[a] SD, standard deviation values in parentheses; ND, not determined.

chance correlation was ruled-out by randomization trials (10 trials yield an averaged $r_{random} < 0.2$; data not shown). Additionally, values for K_i versus R_m show moderate correlation. It is interesting to note that, in the case of Tyr, the ring-centered approach energies are marginally more correlated with K_i than the minimized approach energies— this is in direct contrast with the Trp trajectories where the minimized approach energies are markedly more correlated to K_i. The α4β2 dataset was split into one that includes **8** and **9** (set A) and one that excludes these ligands (set B), due to the fact that their $E_m$values are the most weakly correlated of the study set.

Discussion

In the present work we have established that the cationic moieties of various nAChR ligands interact with aromatic groups to an extent proportional to their receptor binding coefficients. These findings support the hypothesis of Dougherty and Stauffer[42] that π−cation interactions are important in nAChR molecular recognition. Semiempirical energy calculations conducted on ligand−side chain pairs indicate that quantitative differences in ligand binding energy can be predicted. The magnitude of this interaction is significant and often several multiples of kT (at room temperature), but caution must be exercised attributing a physical cause to these observations. The level of theory used to perform these calculations was chosen as a matter of computational efficiency, and we anticipate that they underestimate the extent of the π−cation and other interactions. A higher level of theory, one that takes into account the effects of polarization and correlation, will be required to unravel the relative contributions of ion-multipole, induced multipole, polarization, and charge-

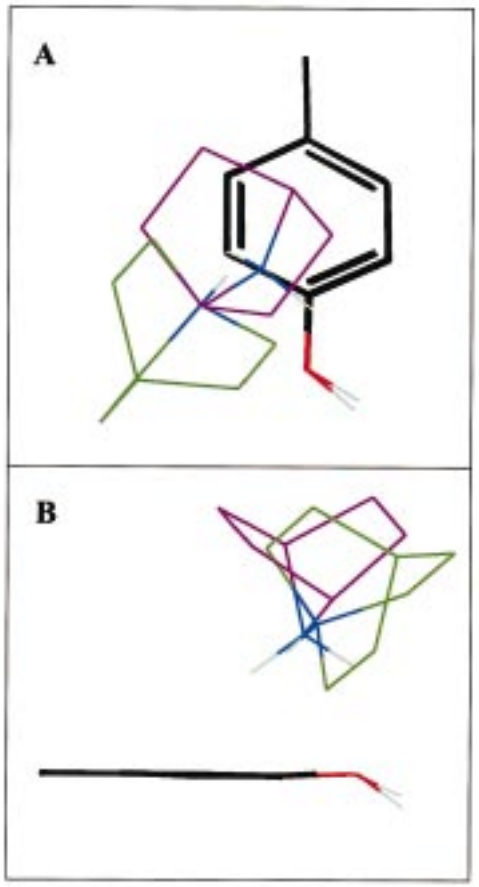

Figure 9. Minimized geometries of **11**−Tyr and **10**−Tyr with the Tyr moieties superimposed: (A) the fragment **11** is purple and the fragment **10** is green; (B) orthogonal view of A.

transfer interactions. Nonetheless, it is likely that the AM1 Hamiltonian *mis*-estimates the interaction similarly across the ligand−side chain pairs described in this study, implying this level of theory should be sufficient for use in quantitative structure−activity studies.

Calculations employing the 'minimized approach' trajectories reveal that the nature of the interaction between cationic ligands and heteroatom-containing amino acids may involve factors beyond electrostatic interaction of π-electrons (δ^-) and cations (+); this conclusion is consistent with the observations of Caldwell and Kollman who attribute only 60% of aromatic−cation interaction to electrostatics.[43] Additionally, Dougherty and co-workers find a correlation between experimental Na^+−aromatic binding enthalpies and ab initio derived electrostatic potentials.[44] But, despite the observed correlation, their calculations fail to account for 12 kcal/mol of the experimental enthalpy throughout the dataset, implying that additional factors contribute. A recent publication by this group has provided exciting additional evidence for the primacy of π−cation interactions in biological molecular recognition. Dougherty and co-workers expressed series of unnatural amino acid mutants of nAChR (binding site αTrp-149). Their activation by acetylcholine was then assessed; a striking correlation between EC_{50} and ab initio calculated interaction energy was observed for the series.[45]

Despite the fact that the semiempirical methodology used in this investigation does not account for polarization, a significant indication of interactions not directly related to the π−cation type emerged. The magnitude of E_m, in all cases, was less for Phe than for Tyr and Trp. Additionally, the ≈2 kcal/mol gained due to heteroatom interaction, measured in the **11−cyclohexanol** experiments, fails to account for these energy differences. We also observe that, upon energy minimization, cationic fragments move toward the aromatic heteroatom, an indication that nonaromatic interactions (perhaps electrostatic in origin) may contribute significantly to the magnitude of interaction *and* the discrimination of ligands. The fact that 2 kcal/mol of favorable energy is gained upon minimization of many *non*protonated ligand−side chain pairs also implies that other factors contribute to the observed interaction. Taken together, these results lead us to an important question—do the contributions to the calculated interaction energy (such as ion-multipole, induced multipole, dispersion, charge-transfer, polarization, etc.) reflect what occurs in the receptor protein? Although the resolution of this issue is a matter of further investigation, it can be said that, in most cases, the values of E_m and R_m show a higher correlation with ligand binding for those trajectories where heteroatom interactions are fully appreciated (i.e. the minimized approach trajectories).

In conclusion, this study provides additional evidence that π−cation interactions are important in the process of nAChR molecular recognition. It is indeed somewhat surprising that such high correlations are found on the basis of semiempirical derived variational energies alone, for other factors such as desolvation free energy, molecular geometry (pharmacophores), and conformational entropy contribute significantly to this process. Future investigations, at higher levels of theory, will undoubtedly unravel sources of this correlation. Nonetheless, E_m and R_m are easily calculated and can be added to the arsenal of QSAR descriptors for use in predictive methodologies and drug design.

References

(1) Dougherty, D. A. cation−pi interactions in chemistry and biology: a new view of benzene, Phe, Tyr, and Trp. *Science (Washington, D.C.)* **1996**, *271*, 163−8.

(2) Kao, P. N.; Dwork, A. J.; Kaldany, R. R. J.; Silver, M. L.; Wideman, J.; Stein, S.; Karlin, A. Identification of the α subunit half-cystine specifically labeled by an affinity reagent for the acetylcholine receptor binding site. *J. Biol. Chem.* **1984**, *259*, 11662−5.

(3) Dennis, M.; Giraudat, J.; Kotzyba-Hibert, F.; Goeldner, M.; Hirth, C.; Chang, J. Y.; Lazure, C.; Chretien, M.; Changeux, J.-P. Amino acids of the *Torpedo marmorata* acetylcholine receptor α subunit labeled by a photoaffinity ligand for the acetylcholine binding site. *Biochemistry* **1988**, *27*, 2346−57.

(4) Abramson, S. N.; Li, Y.; Culver, P. An analogue of lophotoxin that reacts covalently with tyr190 in the alpha subunit of the nicotinic acetylcholine receptor. *J Biol. Chem.* **1989**, *264*, 12666−72.

(5) Galzi, J.-L.; Revah, F.; Black, D.; Goeldner, M.; Hirth, C.; Changeux, J.-P. Identification of a novel amino acid alpha-tyrosine 93 within the cholinergic ligands-binding sites of the acetylcholine receptor by photoaffinity labeling. Additional evidence for a three-loop model of the cholinergic ligand-binding sites. *J. Biol. Chem.* **1990**, *265*, 10430−7.

(6) Middleton, R. E.; Cohen, J. B. Mapping of the acetylcholine binding site of the nicotinic acetylcholine receptor: [^{3}H]nicotine as an agonist photoaffinity label. *Biochemistry* **1991**, *30*, 6987−97.

(7) Tomaselli, G. F.; McLaughlin, J. T.; Jurman, M. E.; Hawrot, E.; Yellen, G. Mutations affecting agonist sensitivity of the nicotinic acetylcholine receptor. *Biophys. J.* **1991**, *60*, 721−7.

(8) Chiara, D. C.; Cohen, J. B. Identification of the amino acids contributing to high and low affinity dTC sites on the Torpedo nAChR. *Biophys. J.* **1992**, *61*, A106.

(9) O'Leary, M. E.; White, M. M. Mutational analysis of ligand-induced activation of the Torpedo acetylcholine receptor. *J. Biol. Chem.* **1992**, *267*, 8360−5.

(10) Czajkowski, C.; Karlin, A. Structure of the nicotinic acetylcholine receptor binding site. *J. Biol. Chem.* **1995**, *270*, 3160−4.

(11) Sine, S. M.; Quiram, P.; Papanikolaou, F.; Kreienkamp, H. J.; Taylor, P. Conserved tyrosines in the alpha subunit of the nicotinic acetylcholine receptor stabilize quaternary ammonium groups of agonists and curariform antagonists. *J. Biol. Chem.* **1994**, *269*, 8808−16.

(12) Fu, D.-X.; Sine, S. M. Competitive antagonists bridge the alpha-gamma subunit interface of the acetylcholine receptor through quaternary ammonium-aromatic interactions. *J. Biol. Chem.* **1994**, *269*, 26152−7.

(13) Prince, R. J.; Sine, S. M. Molecular dissection of subunit interfaces in the acetylcholine receptor. Identification of residues that determine agonist selectivity. *J. Biol. Chem.* **1996**, *271*, 25770−7.

(14) Sugiyama, N.; Boyd, A. E.; Taylor, P. Anionic residue in the alpha-subunit of the nicotinic acetylcholine receptor contributing to subunit assembly and ligand binding. *J. Biol. Chem.* **1996**, *271*, 26575−81.

(15) Cheng, X.; Kumar, S.; Klimasauskas, S.; Roberts, R. J. Crystal structure of the HhaI DNA methyltransferase. *Cold Spring Harbor Symp. Quant. Biol.* **1993**, *58* (DNA and Chromosomes), 331−8.

(16) Novotny, J.; Bruccoleri, R. E.; Saul, F. A. On the attribution of binding energy in antigen−antibody complexes McPC603, D1.3, and HyHEL-5. *Biochemistry* **1989**, *28*, 4735−49.

(17) Sussman, J. L.; Harel, M.; Silman, I. 3-D structure of acetylcholinesterase and complexes of it with anticholinesterase agents. *Jerusalem Symp. Quantum Chem. Biochem.* **1992**, *25* (Membrane Proteins: Structures, Interactions and Models), 161−75.

(18) Ordentlich, A.; Barak, D.; Kronman, C.; Ariel, N.; Segall, Y.; Velan, B.; Shafferman, A.; Contribution of aromatic moieties of tyrosine 133 and of the anionic subsite tryptophan 86 to catalytic efficiency and allosteric modulation of acetylcholinesterase. *J. Biol. Chem.* **1995**, *270*, 2082−91.

(19) Martinez, A.; Abeygunawardana, C.; Haavik, J.; Flatmark, T.; Mildvan, A. S. Conformation and interaction of phenylalanine with the divalent cation at the active site of human recombinant tyrosine hydroxylase as determined by proton NMR. *Biochemistry* **1993**, *32*, 6381−90.

(20) Lin Z.; Johnson, M. E. Proposed cation−pi mediated binding by factor Xa: a novel enzymic mechanism for molecular recognition. *FEBS Lett.* **1995**, *370*, 1−5.

(21) Kier, L. B.; Aldrich, H. S. A theoretical study of receptor site models for trimethylammonium group interaction. *J. Theor. Biol.* **1974**, *46*, 529−41.
(22) Calvarie, P.; Rein, R. Multipole-bond polarizabilities and intermolecular interaction. *Int. J. Quantum Chem.* **1969**, *3*, 537−42.
(23) Holtje, H.-D.; Kier, L. B. Nature of the anionic alpha-site of cholinesterase. *J. Pharm. Sci.* **1975**, *64*, 418−20.
(24) Akoi, K.; Murayama, K.; Nishiyama, H. cation−pi interaction between the trimethylammonium moiety and the aromatic ring within indole-3-acetic acid choline ester, a model compound for molecular recognition between acetylcholine and its esterase: an X-ray study. *Chem. Commun.* **1995**, *331*, 2221−2.
(25) Liljefors, T.; Norrby, P.-O. Ab initio quantum chemical model calculations on the interactions between monoamine neurotransmitters and their receptors. *Alfred Benzon Symp.* **1996**, *39*, 194−207.
(26) Tsigelny, I.; Sugiyama, N.; Sine, S.; Taylor, P. A model of the nicotinic receptor extracellular domain based on sequence identity and residue location. *Biophys. J.* **1997**, *73*, 52−66.
(27) Galzi, J.-L.; Bertrand, D.; Devillers-Thiery, A.; Revah, F.; Bertrand, S.; Changeux, J.-P. Functional significance of aromatic amino acids from three peptide loops of the alpha7 neuronal nicotinic receptor site investigated by site-directed mutagenesis. *FEBS Lett.* **1991**, *294*, 198−202.
(28) Galzi, J.-L.; Changeux, J.-P. Neurotransmitter-gated ion channels as unconventional allosteric proteins. *Curr. Opin. Struct. Biol.* **1994**, *4*, 554−65.
(29) Sine, S. M.; Kreienkamp, H.-J.; Bren, N.; Maeda, R.; Taylor, P. Molecular dissection of subunit interfaces in the acetylcholine receptor: identification of determinants of alpha-conotoxin M1 selectivity. *Neuron* **1995**, *15*, 205−11.
(30) Stewart, J. J. P. MOPAC: a semiempirical molecular orbital program. *J. Comput.-Aided Mol. Des.* **1990**, *4*, 1−105.
(31) Baker, J. An algorithm for the location of transition states. *J. Comput. Chem.* **1986**, *7*, 385−91.
(32) Dewar, M. J. S.; Zoebisch, E. G.; Healy, E. F.; Stewart, J. J. P. Development and use of quantum mechanical molecular models. 76. AM1: a new general purpose quantum mechanical molecular model. *J. Am. Chem. Soc.* **1985**, *107*, 3902−9.
(33) Stewart, J. J. P. Example of the advantage of the BFGS geometry optimizer over the DFP. *Comput. Chem.* **1989**, *13*, 157−8.
(34) Spartan (Version 3), Wavefunction Inc., Irvine, CA.
(35) Hehre, W. J.; Pau, C. F.; Headley, A. D.; Taft, R. W.; Topsom, R. D. A scale of directional substituent polarizability parameters from ab initio calculations of polarizability potentials. *J. Am. Chem. Soc.* **1986**, *108*, 1711−12.
(36) Cerius^2 (Version 3.1), Molecular Simulations Inc., San Diego, CA.
(37) Hirschfelder, J. O.; Meath, W. J. The nature of intermolecular forces. In *Intermolecular Forces (Advances in Chemical Physics XII)*; Hirschfelder, J. O., Ed.; Interscience (J. Wiley and Sons): New York, 1967; pp 5−29.
(38) Marks, M. J.; Collins, A. C. Characterization of nicotine binding in mouse brain andcomparison with the binding of alpha-bungarotoxin and quinuclidinyl benzilate. *Mol. Pharmacol.* **1982**, *22*, 554−64.
(39) Bencherif, M.; Schmitt, J. D.; Crooks, P.; Lovette, M. E.; Fowler, K.; Reeves, L.; Caldwell, W. S.; Lippiello, P. M. The heterocyclic substituted pyridine derivative 2-azabicyclo[2.2.1]hept-5-ene [RJR-2429]: a selective agonist at nicotinic acetylcholine receptors. *J. Pharmacol. Exp. Ther.* **1998**, *284*, 886−94.
(40) Abood, L. G.; Lu, X.; Banerjee, S. Receptor binding characteristics of a tritium-labeled azetidine analogue of nicotine. *Biochem. Pharmacol.* **1987**, *36*, 2337−41.
(41) Sharples, C. G. V. Unpublished results.
(42) Dougherty, D. A. Stauffer, D. A.; Acetylcholine binding by a synthetic receptor: implications for biological recognition. *Science (Washington, D.C.)* **1990**, *250*, 1558−60.
(43) Caldwell, J. W.; Kollman, P. A. cation-π. Interactions: Nonadditive effects are critical in their accurate representation. *J. Am. Chem. Soc.* **1995**, *117*, 4177−8.
(44) Mecozzi, S.; West, A. P., Jr.; Dougherty, D. A. cation−pi interactions in simple aromatics: electrostatics provide a predictive tool. *J. Am. Chem. Soc.* **1996**, *118*, 2307.
(45) Zhong, W.; Gallivan, J. P.; Zhang, Y.; Li, L. T.; Lester, H. A.; Dougherty, D. A. From *ab initio* quantum mechanics to molecular neurobiology: a cation−pi binding site in the nicotinic receptor. *Proc. Natl. Acad. Sci. U.S.A.* **1998**, *21*, 12088−93.

JM990093Z